 CMES, vol.3, no.3, pp.351-365, 2002

Modeling of Electric Double Layer Effects through Pressure-driven Microchannel Flows

E.Y.K. Ng [1] **and S.T. Poh** [2]

Abstract: Advances in microfabrication technology have allowed the use of microchannels in ultra compact, very efficient heat exchangers, which capitalize on the channels large surface area to volume ratio, to transport high heat fluxes with small thermal resistances. One example is the cooling of microchips. However, research into microscale flow and heat transfer phenomena conducted by various researchers provided substantial experimental data and considerable evidence that the behaviour of fluid flow and heat transfer in microchannels without phase change may be different than that which normally occurs in larger more conventional sized channels.

This paper describes a numerical analysis with the use of a finite-volume scheme on the liquid flow and heat transfer in microchannels, with streaming potential as the driving force. The concept of electric double layer (EDL) was introduced to explain the microscale deviation. Governing equations were derived for fully developed rectangular microchannel flows. Towards a realistic modeling of the rectangular microchannels, a conjugate analysis, that solves both the solid and liquid regions, was performed. An additional source term resulting from the EDL effects was introduced in the conventional momentum equation, thereby modifying the flow and heat transfer characteristics. In this work, analyses concerning the effects of ionic concentration and zeta potential and channel dimensions were discussed.

The predicted results showed significant deviations in the velocity and temperature profiles under EDL effects. Friction factors and Nusselt numbers were calculated and compared for both EDL and non-EDL considerations. Stronger deviations were also observed as the aspect ratio decreases, suggesting the importance of EDL in microscale liquid flow.

keyword: EDL effects, pressure-driven flows, microchannel, simulation, FVM.

[1] College of Engineering
School of Mechanical and Production Engineering
Nanyang Technological University
50 Nanyang Avenue
Singapore 639798.

[2] R&D Engineer, MSC Group
Inc., Milling Systems & Concepts Ltd.
31 Gul Avenue, Singapore 629669.

Nomenclature

c_p	Fluid specific heat
D_h	Microchannel hydraulic diameter
ΔP	Microchannel pressure drop
f	Fully developed friction factor
k	Fluid thermal conductivity
L	Channel length
μ	Fluid viscosity
Nu	Fully developed Nusselt number
Nu_x	Local Nusselt number
Pr	Prandlt number
q''	Wall heat flux
θ	Non-dimensional temperature
Re	Reynolds number
U	Channel flow velocity

1 Introduction

The design of high-speed, high-power integrated circuits and systems is often constrained by thermal considerations. There is a contradictory requirement for high rates of heat dissipation with low allowable temperature rise. Heating rates on the order of 10 W/cm^2 are commonly produced and the allowable temperature rise is usually limited to approximately 80 $^\circ$C above a 20 $^\circ$C ambient. In this decade however, the allowable temperature rise is expected to decrease somewhat, and the heat dissipation rate in the range of 200 to 1000W/cm^2. Hence, innovative cooling techniques will be required to fulfill these specifications and one such method is the use of forced convection heat spreaders called microchannel heat sinks. A microchannel heat sink is a structure with

numerous channels and fins arranged parallel to one another and very close to the heated surface. The dissipated heat passes through the heat sink by conduction and to the coolant by forced convection. The coolant is usually a liquid rather than a gas and the flow is usually single phase rather than two-phase. With the advancement of micromachining techniques, constructing such small but highly efficient micro heat exchangers is feasible.

Tuckerman and Pease (1981) first introduced the concept of a microchannel heat sink at Stanford University. Other researchers' efforts are summarized in Ng and Poh (1999). Microchannel array has been found effective in cooling electronic devices by Yang and Li (1997). The current work intends to carry out a numerical simulation of the flow and heat transfer in a microchannel array with unidirectional flow condition in order to obtain the flow field and the temperature distribution. The numerical scheme is based on the method by Patankar (1991). This classical structured grid finite volume approach was chosen due to its simplicity in implementing the scheme though some recent advancements in unstructured adaptive meshing and the latest meshless methods have been reported. The meshless finite point approach by Wordelman, Aluru, and Ravaioli (2000) held promise in terms of grid enhancement and for solving problems where arbitrary point insertion is important. Ngo and Tamma (2000) proposed an alternative meshless method (not really totally meshless) for heat transfer computations. The recent Meshless Local Petrov-Galerkin (MLPG) method with upwinding has been demonstrated with a great potential in solving the boundary value problems such as the convection-dominated fluid mechanics by the Atluri's group in UCLA [Kim and Atluri (2000), Lin and Atluri (2000)(2001), Atluri and Shen (2002a)(2002b)]. In brief, the meshless method is an alternative to the well-known finite element method (FEM). Both methods are based on the discretization of the variational formulation of partial differential equations. If the (FEM) needs to generate a mesh of elements, a meshless method would be easier to use as it deals only with a cloud of nodes. The approximation is computed on domains of influence, which are generated automatically. This property appears to be a major advantage when thinking about the generation of industrial finite element meshes which is a task requiring important human and computational efforts. The meshless methods are well suited for the numerical computation of the PDF. It is a new method, and is a hot research area in the numerical world. It is not so common in the industrial application yet. Unstructured adaptive meshing with finite volume is more popular since the automated methods for generating both structured and unstructured meshes have been available for many years. Structured or curvilinear grids, characterized by their regular lattice structure, are ideal for finite difference approaches, where this approach can take advantage of the regular nature of the grid for fast identification of neighboring cells. Unstructured meshes, on the other hand, are ideal for finite element simulation and finite volume method over irregular domains and complex geometry. Adaptive mesh can automatically refine the mesh where the sharp physical property gradient occurs. However, automated unstructured mesh generation techniques tend to rely heavily on complex data structures and heuristic computational algorithms. Generally, the above two approaches can easily be implemented on complex domain, avoiding the complicated mesh generation. But much effort has to be done in the node index and data structures. Moreover, the boundary condition may need to be treated carefully.

2 Theoretical formulation

In microscale flow, deviations in trends are likely to be caused by interfacial effects such as the electric double layer (EDL) which has negligible thickness in macroscale flow. Most solid surfaces have electrostatic charges i.e. an electrical surface potential. If the liquid contains very small amounts of ions, the electrostatic charges on the solid surface will attract the counterions in the liquid to establish an electrical field. The arrangement of the electrostatic charges on the solid surface and the balancing charges is called the EDL [Probstein (1994)]. Because of the electrical field, the ionic concentration near the solid surface is higher than that in the bulk liquid. In compact layer, which is about 0.5 nm thick, the ions are strongly attracted to the wall surface and are immobile. In diffuse double layer, the ions are affected less by the electrical field and are mobile. The thickness of the diffuse EDL ranges from a few nanometers up to several hundreds of nanometers, depending on the electric potential of the solid surface, the bulk ionic concentration and other properties of the liquid. When a liquid is forced through a microchannel under hydrostatic pressure, the ions in the mobile part of the EDL are carried towards one end. This causes an electric current,

called streaming current, to flow in the direction of the liquid flow. The accumulation of ions downstream sets up an electrical field with an electrical potential called the streaming potential. This field causes a conduction current to flow back in the opposite direction. When conduction current is equal to the streaming current a steady state is reached. It is easy to understand that, when the ions are moved in the diffuse double layer, they pull the liquid along with them. However, the motion of the ions in the diffuse double layer is subjected to the electrical potential of the double layer. Thus the liquid flow and heat transfer are affected by the presence of the EDL. In macroscale flow, these interfacial electro-kinetic effects are negligible as the thickness of the EDL is negligible compared to the hydraulic radius of the flow channel. However, in microscale flow the EDL thickness is comparable to the hydraulic radius of the flow channel. For submicron capillaries the EDL thickness may even be larger than the radius of the capillary. Thus EDL effects must be considered in the studies of microscale flow and heat transfer. The schematic representation of the EDL at the channel is shown in Figure 1.

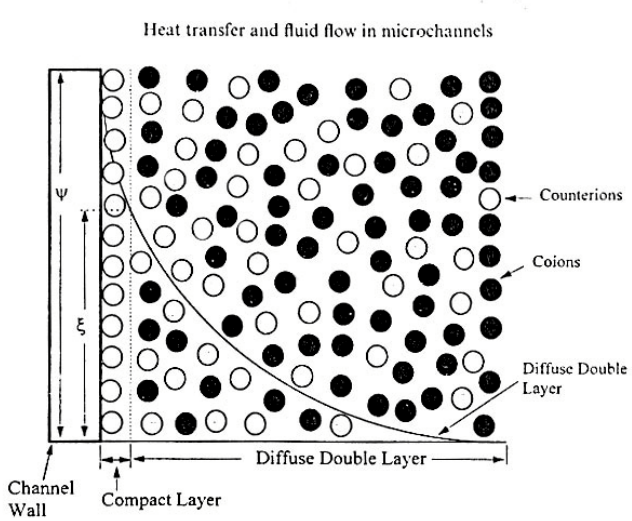

Figure 1 : Schematic representation of the electric double layer at the channel wall [from Mala, Li and Dale (1997)]

Here, the effects of EDL at the solid-liquid interface on fluid flow and heat transfer through a microchannel is investigated. The numerical solution of the 2D, non-linear, 2nd order Poisson-Boltzmann equation is used to describe the EDL field. The addition of the electrical body force, resulting from the double layer field, to the equation of motion results in a modified velocity distribution upon solving for steady state flow.

2.1 Surface electrostatic potential

As the cross-sections of microchannels are close to rectangular shape, the Poisson-Boltzmann equation is required to describe the existing of EDL field. The partial differential equation is solved numerically to obtain a complete solution.

Consider a liquid phase containing positive and negative ions in contact with a planar positively or negatively charged surface. The surface bears a uniform electrostatic potential, which decreases as one proceeds out into the liquid. Far away from the wall, the concentration of the positive and negative ions is equal. The electrostatic potential, Ψ at any point near the surface is related to its net number of electrical charges per unit volume, ρ_e in the neighborhood of the point, which measures the excess of the positive ions over negative ions or vice versa.

According to the theory of electrostatics, the relationship between Ψ and ρ_e is given by the Poisson's equation, which for a rectangular channel with width W_c and depth H_c as depicted in Figure 2.

$$\frac{\partial^2\Psi}{\partial X^2}+\frac{\partial^2\Psi}{\partial Y^2}=-\frac{\rho_e}{\varepsilon\varepsilon_o} \tag{1}$$

where ε is the dielectric constant of the medium and ε_o is the permittivity of a vacuum.

Assuming that the equilibrium Boltzmann distribution equation is applicable, which implies uniform dielectric constant, the number concentration of the type-i ion in a symmetric electrolyte solution is of the form:

$$n_i = n_{i0}\exp\left(-\frac{z_i e\Psi}{k_b T}\right) \tag{2}$$

where

z_i = valence of type-i ions
k_b = Boltzmann constant = 1.3805 x 10^{-23} J mol^{-1} K^{-1}
T = absolute temperature (K)
e = electron charge = 1.6021 x 10^{-19} C
n_{i0} = bulk concentration of type-i ions

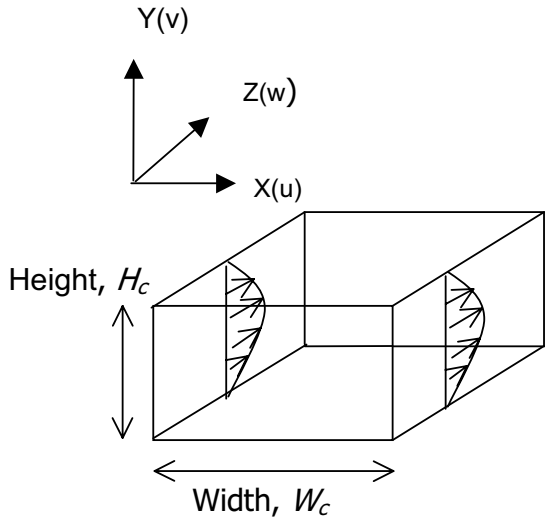

Figure 2 : Schematic of a rectangular microchannel

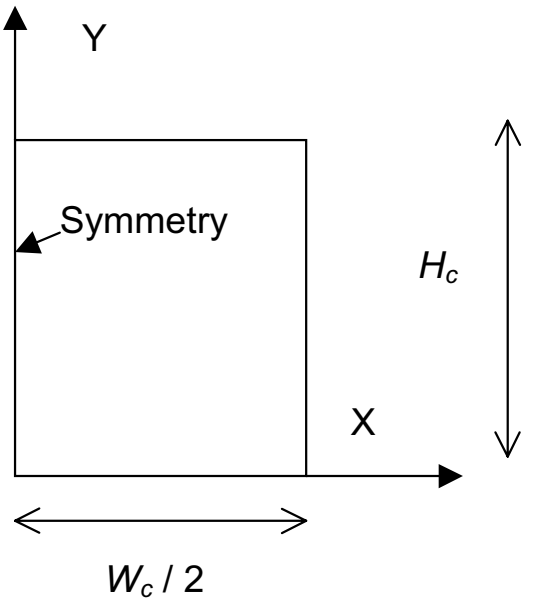

Figure 3 : Computational domain

The net charge density in a unit volume of the fluid is given by:

$$\rho_e = \left(n^+ - n^-\right) ze = -2n_0 ze \sinh\left(\frac{ze\Psi}{k_b T}\right) \tag{3}$$

Subsequently, a nonlinear second-order two-dimensional Poisson-Boltzmann equation has the form of:

$$\frac{\partial^2 \Psi}{\partial X^2} + \frac{\partial^2 \Psi}{\partial Y^2} = \frac{2n_0 ze}{\varepsilon\varepsilon_0} \sinh\left(\frac{ze\Psi}{k_b T}\right) \tag{4}$$

Using the variables defined as follows:

$$x = \frac{X}{D_h} \quad y = \frac{Y}{D_h} \quad \psi = \frac{ze\Psi}{k_b T} \quad D_h = \frac{4H_c W_c}{2(H_c + W_c)}$$

where x is the non-dimensional X-coordinate, y is the non-dimensional Y-coordinate, D_h is the hydraulic diameter of the channel and ψ is the non-dimensional surface electrostatic potential. The non-dimensional form of the Poisson-Boltzmann equation is thus given as:

$$\frac{\partial^2 \psi}{\partial x^2} + \frac{\partial^2 \psi}{\partial y^2} = \kappa^2 \sinh\left(\frac{ze\Psi}{k_b T}\right) \tag{5}$$

where

$$\kappa = D_h \beta \qquad \beta = \left(\frac{2n_0 z^2 e^2}{\varepsilon\varepsilon_0 k_b T}\right)^{\frac{1}{2}}$$

β is called the Debye-Huckel parameter, while $(\beta)^{-1}$ is the characteristic thickness of the EDL. Note that a small κ implies a small ratio of $D_h (\beta)^{-1}$ which is for the case of microchannel flow.

Due to the symmetry of a rectangular microchannel, one half of the rectangular microchannel is considered for the computational domain as shown in Figure 3. The non-dimensional Poisson-Boltzmann equation is subjected to the following boundary conditions:
At

$$\begin{aligned} x &= 0, & \frac{\partial \psi}{\partial x} &= 0 \\ x &= \frac{\overline{W}}{2}, & \psi &= \overline{\xi}_2 \\ y &= 0, & \psi &= \overline{\xi}_1 \\ y &= \overline{H}, & \psi &= \overline{\xi}_1 \end{aligned}$$

where

$\overline{W} = \dfrac{W}{D_h}$ = nondimensional microchannel width

$\overline{H} = \dfrac{H}{D_h}$ = nondimensional microchannel height

$\overline{\xi}_i = \dfrac{ze\xi_i}{k_b T}\ (i = 1, 2)$ = nondimensional zeta potential at channel walls

In the following analysis, all wetted surfaces of the microchannel are assumed to have same zeta potential.

2.2 Momentum equations

A reduced Navier-Stokes equation, which includes the EDL effect, can be written as:

$$\frac{\partial^2 u}{\partial X^2}+\frac{\partial^2 u}{\partial Y^2}=\frac{1}{\mu_f}\frac{dP}{dZ}-\frac{1}{\mu_f}E_z\rho_e(X,Y) \tag{6}$$

Neglecting gravity effect, the body force F is caused by the action of the induced electrical field, E_z on the net charge density and ρ_e in the electrical double layer region with $F=E_z\rho_e$.

Non-dimensionalizing using the following parameters:

$$\overline{u}=\frac{u}{U} \qquad \overline{P}=\frac{P-P_0}{\rho U^2}$$

$$z=\frac{Z}{D_h Re_0} \qquad \frac{d\overline{P}}{dz}=\frac{D_h Re_0}{\rho U^2}\frac{dP}{dZ}$$

$$\overline{E}_z=\frac{E_z D_h Re_0}{\xi_0} \qquad Re_0=\frac{\rho D_h U}{\mu}$$

The non-dimensional equation of motion is thus:

$$\frac{\partial^2 \overline{u}}{\partial x^2}+\frac{\partial^2 \overline{u}}{\partial y^2}=\frac{d\overline{P}}{dz}-\frac{\xi_0}{\rho U^2}\overline{E}_z\rho_e(x,y) \tag{7}$$

Substituting the local net charge density, Eq. (7) can be expressed as:

$$\frac{\partial^2 \overline{u}}{\partial x^2}+\frac{\partial^2 \overline{u}}{\partial y^2}=\frac{d\overline{P}}{dz}+\overline{G}_1\overline{E}_z\sinh\psi(x,y) \tag{8}$$

with

$$\overline{G}_1=\frac{2zen_0\xi}{\rho_f U^2};\quad \rho_f=\text{ density of fluid} \tag{9}$$

The boundary conditions include:

$$x=0 \qquad \frac{\partial \overline{u}}{\partial x}=0 \quad \text{symmetrical condition}$$

$$x=\frac{W_c}{2D_h} \quad \overline{u}=0 \quad ; \quad \text{no-slip condition}$$

$$y=\frac{H_c}{D_h} \quad \overline{u}=0 \quad ; \quad y=0 \quad \overline{u}=0$$

When a liquid is forced through a microchannel under a hydrostatic pressure difference and at steady state in which the conduction current is equal to the streaming current with $I_c+I_s=0$

The electrical streaming current is of the form [Hunter (1981)]:

$$I_s=D_h^2 U\int_{x=0}^{\frac{W_c}{D_h}}\int_{y=0}^{\frac{H_c}{D_h}}\overline{u}(x,y)\,\rho_e(x,y)\,dxdy \tag{10}$$

On the other hand, the electrical conduction current is expressed as:

$$I_c=\lambda_t E_z A_c=\frac{\lambda_t H_c W_c \xi}{D_h Re_0}\overline{E}_z \tag{11}$$

where λ_t = electrical conductivity of the fluid per unit length

As a result, the non-dimensional induced field strength is given as:

$$\overline{E}_z=\frac{D_h^2}{H_c W_c}\overline{G}_2 Re_0\int_{x=0}^{\frac{W_c}{D_h}}\int_{y=0}^{\frac{H_c}{D_h}}\overline{u}(x,y)\sinh(x,y)\,dxdy \tag{12}$$

where

$$\overline{G}_2=\frac{2zen_0 D_h U}{\lambda_t \xi_0}$$

In the conventional fluid mechanics, the friction factor for the flow through rectangular channels is defined as:

$$f=\frac{-\frac{dP}{dZ}\frac{D_h}{4}}{\frac{\rho_f u_{ave}^2}{2}}=\frac{-\frac{d\overline{P}}{dz}}{2Re_0\overline{u}_{ave}^2} \tag{13}$$

where

$$\frac{d\overline{P}}{dz} = \frac{D_h \frac{dP}{dZ}}{\mu_f U}$$

The friction constant, C_f is thus given as:

$$C_f = fRe = \frac{-\frac{d\overline{P}}{dz}}{2Re_0 \overline{u}_{ave}^2}\left[\frac{\rho_f D_h u_{ave}}{\mu_f}\right] = \frac{-\frac{d\overline{P}}{dz}}{2\overline{u}_{ave}^2} \quad (14)$$

where

$$Re = \frac{\rho_f D_h u_{ave}}{\mu_f}$$

2.3 Energy equation

For a steady state, fully developed, laminar incompressible flow in a microchannel, the energy equation for the coolant is given as:

$$u\frac{\partial T}{\partial Z} = \alpha_f\left(\frac{\partial^2 T}{\partial X^2} + \frac{\partial^2 T}{\partial Y^2} + \frac{\partial^2 T}{\partial Z^2}\right) + \frac{\mu_f}{\rho_f C_p}\left[\left(\frac{\partial u}{\partial X}\right)^2 + \left(\frac{\partial u}{\partial Y}\right)^2\right] \quad (15)$$

where T, α_f and C_p are the temperature, thermal diffusivity and the specific heat capacity of the cooling liquid.

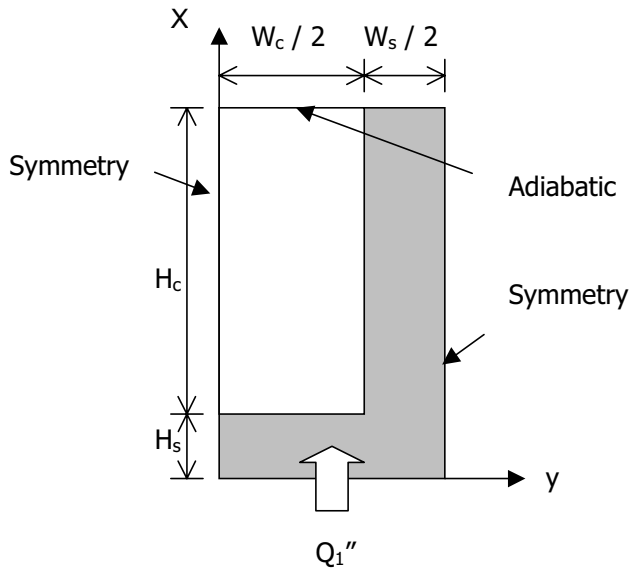

Figure 4 : Schematic of thermal boundary conditions imposed on solution domain

Figure 4 shows the microchannel solution domain with its thermal boundary conditions. Microchannels are normally capped with a cover plate that is typically made out of a relatively low conductivity material, such as glass. Its conductivity is about two order lower than that of silicon, hence adiabatic condition is assumed at the top wall as its contribution is negligible. Uniform heat flux Q_1'' are applied to the channel's bottom wall. Symmetry conditions are applied to both the left and right boundaries.

For fully developed internal flow subjected to constant heat flux, the temperature gradient along the axial direction is constant i.e. all temperatures rise linearly with Z at the same rate. Therefore,

$$\frac{\partial T}{\partial Z} = \frac{\partial T_b}{\partial Z} = \text{constant} \quad (16)$$

$$\frac{\partial^2 T}{\partial Z^2} = 0 \quad (17)$$

where T_b is the bulk fluid temperature

Hence, the energy equation is reduced to:

$$\rho C_P u\frac{\partial T_b}{\partial Z} = k\left(\frac{\partial^2 T}{\partial X^2} + \frac{\partial^2 T}{\partial Y^2}\right) + \mu\left[\left(\frac{\partial u}{\partial X}\right)^2 + \left(\frac{\partial u}{\partial Y}\right)^2\right] \quad (18)$$

Applying overall heat balance within the microchannel, the temperature gradient along the axial direction is expressed via:

$$Q_1''\left(\frac{W_c}{2} + \frac{W_s}{2}\right) = \rho u_{\text{ave}} A C_P \frac{dT_b}{dZ} \quad (19)$$

where W_s is the channel fin width.

A is the effective cross-sectional area normal to flow direction = $H_c W_c/2$, or,

$$\frac{dT_b}{dZ} = \frac{Q_1'' L'}{\rho u_{\text{ave}} A C_P} \quad (20)$$

with

$$L' = \frac{W_c + W_s}{2} \quad (21)$$

Substituting Eq. (20) into Eq. (18) gives

$$\frac{Q_1'' L'}{\rho A C_P}\frac{u}{u_{\text{ave}}} = \frac{k}{\rho C_P}\left(\frac{\partial^2 T}{\partial X^2} + \frac{\partial^2 T}{\partial Y^2}\right) + \frac{\mu}{\rho C_P}\left[\left(\frac{\partial u}{\partial X}\right)^2 + \left(\frac{\partial u}{\partial Y}\right)^2\right]$$

(22)

$$\text{By defining } z = \frac{Z}{D_h} \text{ and } \theta = \frac{(T - T_b)\,k}{Q_1'' L'} \tag{23}$$

Equation (22) can then be written as:

$$\left(\frac{\partial^2\theta}{\partial x^2} + \frac{\partial^2\theta}{\partial y^2}\right) + \mathrm{Pr}\,\mathrm{Ec}\left[\left(\frac{\partial \overline{u}}{\partial x}\right)^2 + \left(\frac{\partial \overline{u}}{\partial y}\right)^2\right] - \frac{D_h^2}{A}\frac{u_0}{u_{\text{ave}}}\overline{u} = 0 \tag{24}$$

where

$$\mathrm{Pr} = \frac{\mu C_P}{k} \quad Ec = \frac{u_0^2 k}{C_P Q_1'' L'}$$

The boundary conditions that applied to the solution domain are:

$$\begin{aligned} y &= 0 & \frac{\partial\theta}{\partial y} &= \frac{D_h}{L'} \\ y &= \frac{H_s + H_c}{D_h} & \frac{\partial\theta}{\partial y} &= 0 \\ x &= 0 & \frac{\partial\theta}{\partial x} &= 0 \\ x &= \frac{L'}{D_h} & \frac{\partial\theta}{\partial x} &= 0 \end{aligned} \tag{25}$$

3 Numerical algorithm

The details of the numerical scheme, discretization equation, treatment of boundary conditions, grid used and control volume generation are based on the classical finite volume approach as described in chapter 5 by Patankar (1991).

For a two-dimensional problem, as used for fully-developed flow cases, the basic construction of the control volumes and the grid points are placed at the centers of the control volumes. A grid point is linked to its four neigbouring grid points through the four faces of the control volume. A non-uniform grid was employed in the scheme. The grid adjacent to the solid wall is clustered in order to capture the gradient change of electrical potential, flow and heat transfer variables. However, the grid in the solid region is not as fine as compared to liquid flow region due to its relatively larger thermal conductivity resulting in small temperature gradient across the solid domain. Grid dependency test was carried out by first running test cases in 13 x 8 elements. The test cases were then carried out in increasing number of elements namely in multiples of two, three and four. However, due to limited CPU time and memory, the tests were terminated at multiples of four. Results of the grid invariance study showed that the results obtained leveled off after multiples of two. Hence, the grid with 26 x 16 fluid and solid elements in x, y directions respectively were chosen as the final grid.

The non-dimensional Poisson-Boltzmann, momentum and energy equations are basically the differential equations and thus can be represented by appropriate general differential equations. Two types of boundary treatment namely the lower-order and the higher-order treatments are used.

4 Computational modeling procedure

For simple channel flow analysis, the analysis of heat transfer mechanism can be performed by assuming that the heat flux along the channel height is uniform. This approximation follows the works of Tuckerman (1981) and Samalam (1989) who used the classical fin analysis that assumes uniform heat transfer coefficient along the channel wall. However, in order to obtain a more realistic understanding of the heat transfer mechanism as pointed out by Weisberg, Bau and Zemel (1992), a conjugate analysis that consists of determination of the temperature fields in both the solid substrate and the fluid region must be solved simultaneously. The microchannel flow simulations presented in this work were conducted to investigate the following two aspects:

- Effect of Ionic Concentration, c_0 (M) and Zeta Potential, ξ (mV)
- Effect of Different Geometric Parameters: Aspect Ratios, H_c/W_c by varying the corresponding geometric, fluid and parametric parameters.

4.1 Numerical procedure

The solution procedure employed is a combination of the line-by-line method and a block correction scheme described in more details in Patankar (1991), to which the interested reader is referred. To sum up briefly, the non-dimensional governing equations as detailed in section 2.0 were solved using the finite volume method. The discretization equations were obtained by converting the differential equations into the algebraic equations. Discretization equations include the unknown values of the

Table 2 : Description of test cases for single fully developed channel flows

Case #.	Zeta potential, ξ (mV)	ΔP (atm)	Heat flux, q'' (W/m^2)	Ionic concentration, c_0 (M)
A1	200	4	1 x 10^5	10^{-8}
A2	150	4	1 x 10^5	10^{-8}
A3	75	4	1 x 10^5	10^{-8}
A4	50	4	1 x 10^5	10^{-8}
A5	200	4	1 x 10^5	10^{-7}
A6	150	4	1 x 10^5	10^{-7}
A7	75	4	1 x 10^5	10^{-7}
A8	50	4	1 x 10^5	10^{-7}
A9	200	4	1 x 10^5	10^{-6}
A10	150	4	1 x 10^5	10^{-6}
A11	75	4	1 x 10^5	10^{-6}
A12	50	4	1 x 10^5	10^{-6}
A13	200	4	1 x 10^5	10^{-5}
A14	150	4	1 x 10^5	10^{-5}
A15	75	4	1 x 10^5	10^{-5}
A16	50	4	1 x 10^5	10^{-5}

variables concerned (e.g. $\overline{u}$, θ) at selected discrete locations arranged on grid points. A small control-volume is then generated around each grid point and by integrating the differential equation over such control volume, one obtains the discretization equations. The non-linear Poisson-Boltzmann equation was first solved to yield the electrical potential field. Subsequently, the momentum equation, with the inclusion of the electrical body force as the source term in the R.H.S., was solved for the velocity field. Finally, the energy equation under the affected velocity profile was solved to obtain the temperature fields.

4.2 Geometry and test cases

At present, a total of 16 test cases were conducted to investigate the effect of ionic concentration and zeta potential on microchannel flows. Each of the cases was limited to the following channel dimensions as presented in Tables 1 and 2.

Table 1 : Microchannel geometry of single-layer conjugate flow

Channel Height, H_c	20 μm
Channel Width, W_c	30 μm
Substrate Width, W_s	8 μm
Substrate Height, H_s	6 μm
Channel Length, L	1000 μm

Next, additional 18 test cases (Table 3) were conducted to investigate microchannel flow with and without the consideration of EDL under the influence of geometric parameters. Aspect ratios, H_c/W_c are varied which in these cases, the width is maintained constant while varying the height of the microchannel and the substrate dimensions remained unchanged as indicated in Table 1.

The liquid used for all these (16+18) test cases is a dilute aqueous 1:1 potassium chloride (KCl) solution whose properties at room temperature are summarized as [Weast, Astle and Beyer (1986)]:

Dielectric constant	80.0
Dynamic viscosity (kg/ms)	0.9E-3
Density (kg/m^3)	997.0
Thermal conductivity (W/mK)	0.605

Silicon is used as the solid substrate whose thermal conductivity is k_s = 148.0 W/mK.

Comparisons were made between the friction coefficient values of the conventional fully developed flow in rectangular ducts (single channel) where water is used as the working fluid. The analytical data were obtained from Shah and London (1978). The computed numerical values of (fRe) (Eq. 15) agree with the exact solution well within 1% as presented in Table 4.

Table 3 : Description of test cases for single-layer conjugate channel

Case No.	Height, H_c (μm)	Width, W_c (μm)	ξ(mV)	C_0(M)	ΔP (atm)	Aspect ratio
B1	20	30	200	10^{-8}	4	0.667
B2	30	30	200	10^{-8}	4	1.0
B3	40	30	200	10^{-8}	4	1.333
B4	60	30	200	10^{-8}	4	2.0
B5	80	30	200	10^{-8}	4	2.667
B6	100	30	200	10^{-8}	4	3.333
B7	20	30	150	10^{-6}	4	0.667
B8	30	30	150	10^{-6}	4	1.0
B9	40	30	150	10^{-6}	4	1.333
B10	60	30	150	10^{-6}	4	2.0
B11	80	30	150	10^{-6}	4	2.667
B12	100	30	150	10^{-6}	4	3.333
B13	20	30	Conventional		4	0.667
B14	30	30	Conventional		4	1.0
B15	40	30	Conventional		4	1.333
B16	60	30	Conventional		4	2.0
B17	80	30	Conventional		4	2.667
B18	100	30	Conventional		4	3.333

Table 4 : Comparisons between numerical and exact solutions of fRe

No.	Aspect ratio	Numerical result (a) (fRe)	Shah & London (1978) (b) (analytical fRe)	Error [(a-b)/b]x100%
1	1.0	14.11	14.22708	0.82%
2	1.333	14.32	14.4757	1.076%
3	1.5	14.59	14.71184	0.828%
4	2.0	15.41	15.54806	0.888%
5	3.333	17.34	17.51209	0.983%

Comparisons were also made between the non-dimensional velocity field obtained from the classical expressions for a fully developed laminar water flow in a rectangular duct [Weisberg, Bau and Zemel (1992)] and that of the current code. The parameters used in the comparison are listed in Table 5.

Table 5 : Parameters used for comparison of velocity field

Height, H_c	60μm
Width, $2W_c$	30μm
Length	1000μm
Pressure difference	4atm

The classical expression for the non-dimensional velocity field where $H_c > 2W_c$ is expressed as [Shah and London (1978)]:

$$u(x,y) = \frac{48}{\pi^3 \left[1 - \frac{96}{\pi^5 w_c} \sum_{i=1,3,5,\ldots}^{\infty} \frac{\tanh(i\pi w_c)}{i^5}\right]} \cdot \sum_{i=1,3,5,\ldots}^{\infty} (-1)^{\frac{i-1}{2}} \left[1 - \frac{\cosh(i\pi x)}{\cosh(i\pi w_c)}\right] \frac{\cosh(i\pi y)}{i^3} \qquad (26)$$

The non-dimensional velocity fields from classical expressions and current prediction are included in Figures 5 and 6 respectively.

The velocity and length scales used in the classical expressions are the cross-sectional averaged velocity, u_{ave}, and the channel height whereas they are unity and hydraulic diameter of the channel in the current code respectively. Hence, for ease of comparison, the velocity

Table 6 : Non-dimensional velocity values at various coordinates for classical expressions and numerical code

No.	XX-coordinate	YY-coordinate	Classical	Numerical	% Error
1	0	0	1.9861	1.9675	0.936%
2	0	0.4	0.9857	0.9848	0.091%
3	0	0.31	1.4878	1.4772	0.712%

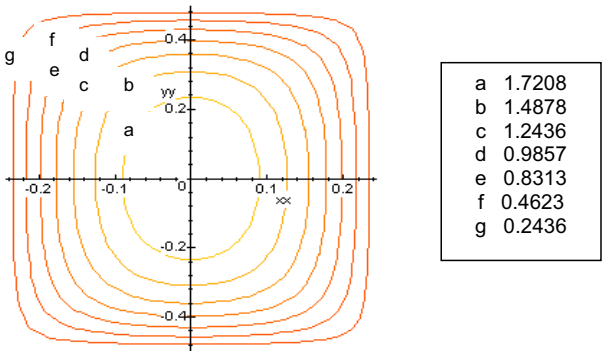

Figure 5 : Non-dimensional velocity profile from classical expressions

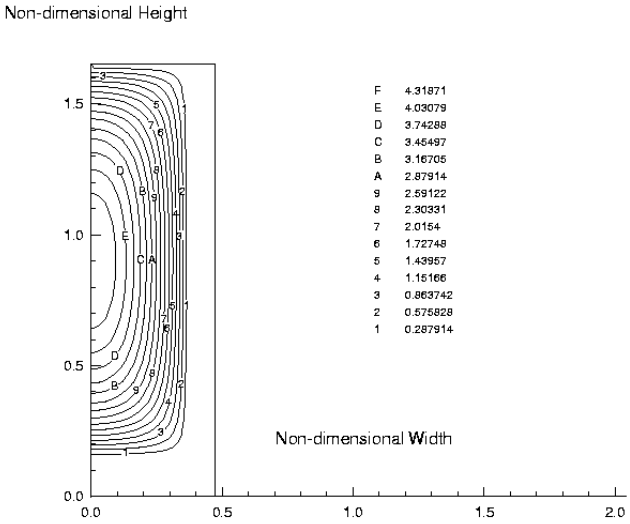

Figure 6 : Non-dimensional velocity profile from current code

scale in the code is changed to u_{ave}. Table 6 shows the non-dimensional velocity values at various coordinates. The coordinate system in the table is based on Figure 2. The errors are well within 0.9%.

5 Results and discussion

5.1 Effect of ionic concentration and zeta potential

5.1.1 Non-dimensional electrical potential distribution

As observed from the electrical potential profile plots (e.g. Figures 7 and 8), the proximity of the contour lines shows that the EDL field exists strongly close to the microchannel wall. Note that there is no EDL field in the solid region hence the zero values throughout the solid region. The EDL effect is more obvious if the EDL field is able to extend to a larger portion of the fluid. This is so for a lower concentrated solution (e.g. 10^{-8}M of Figure 8 vs. 10^{-5}M of Figure 7 for 200mV). A similar trend is also observed for a higher zeta potential. However, the effect of concentration parameter has a dominant effect than zeta potential judging from the higher degree of distortion it has on the EDL field.

5.1.2 Non-dimensional velocity contour distribution

Comparing the velocity profiles of microchannel flow with and without EDL effects as presented in Figures 9, 10, and 11. The EDL field results in a reduction of the global velocity field. The fluid velocity approaches zero near the microchannel wall due to the EDL field. Also, the maximum velocity attained at the center of the microchannel under EDL effects is lower than that without the inclusion of the EDL and the solid region has zero fluid velocities as expected.

It is further observed that lower concentrated solutions (Figures 9 vs. 10) had lower value of velocity distribution. This is also true for higher zeta potential systems. Therefore, the stronger the EDL effect, the larger the influence on the velocity profile would be as can be seen by the modified momentum equation that includes the electrical body force as EDL effects. The lower the ionic concentration, the smaller the Debye-Huckel parameter. Hence, a larger EDL thickness.

With the reduction of the absolute magnitude of velocity, the mean velocity will decrease also under the electroviscous effects. This implies a reduced volumetric flow rate as shown in Figure 12. The effect is greater for a lower ionic concentration of the electrolyte solution and

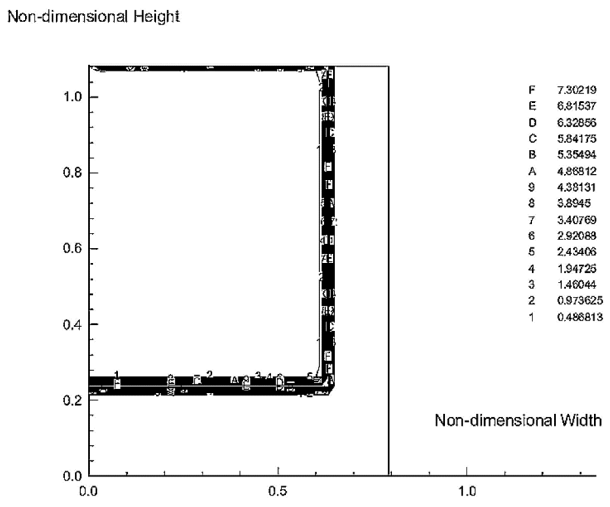

Figure 7 : Non-dimensional EDL distribution (200mV, 10^{-5}M)

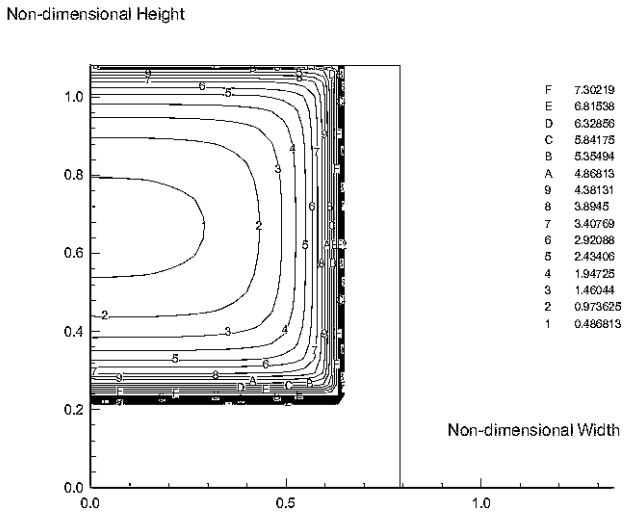

Figure 8 : Non-dimensional EDL distribution (200mV, 10^{-8}M)

also for a higher zeta potential.

The effects of EDL on the friction coefficient (f*Re) are represented in Figure 13. The friction coefficient increases as the ionic concentration decreases and the zeta potential increases. In short, the presence of the EDL increases the friction coefficient from the conventional value.

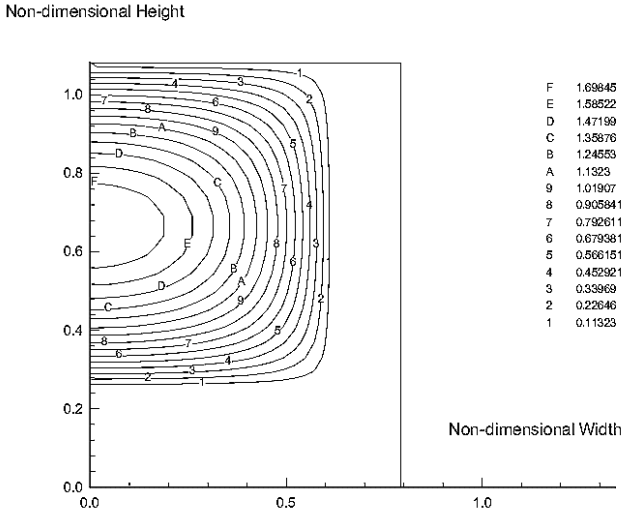

Figure 9 : Non-dimensional velocity distribution (75mV, 10^{-5}M)

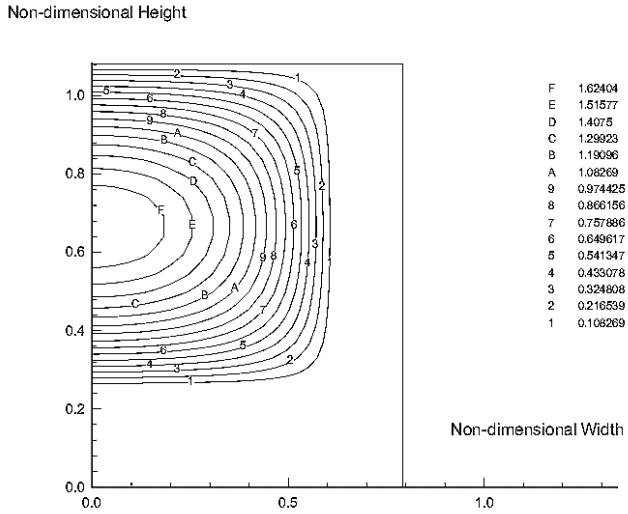

Figure 10 : Non-dimensional velocity distribution (75mV, 10^{-7}M)

5.1.3 Non-dimensional temperature contour distribution

Solving numerically a conjugate heat transfer problem consists of the determination of the temperature fields in both the solid substrate and the fluid region. From the isotherm plots (not included here), the temperature profile is significantly affected by the presence of the EDL field as it changes the velocity flow profile in the microchannel. In general, the presence of the electroviscous effects increases the temperature of the fluid in the microchannel. The boundary between the solid and

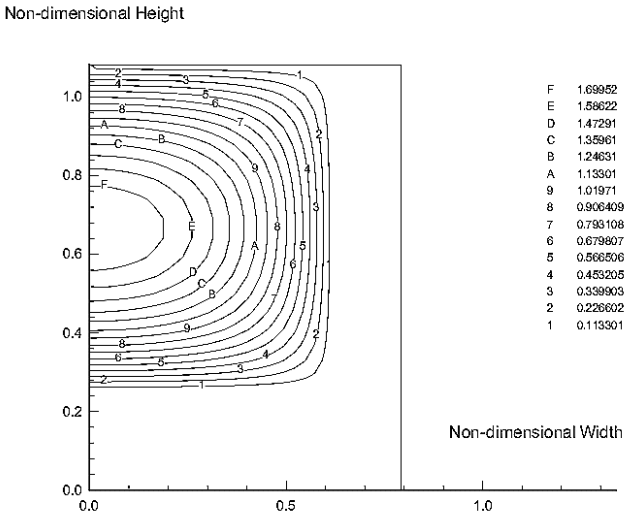

Figure 11 : Non-dimensional velocity distribution (Conventional)

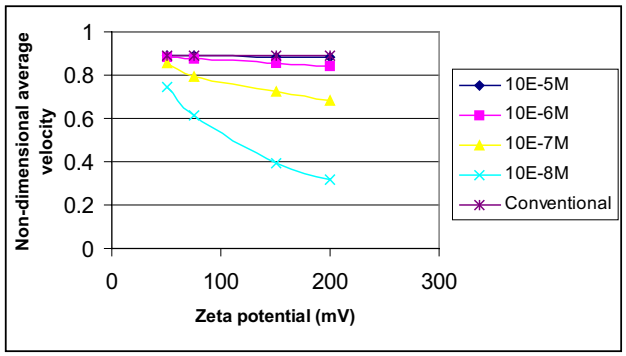

Figure 12 : Dimensionless average velocity vs. zeta potential for various ionic concentrations

the liquid is clearly visible due to the large, discontinuous step-change in the temperature gradient at this interface. Due to the high thermal conductivity of solid, the temperature gradients in the solid substrate are relatively small and the temperature distribution resembles an almost isothermal distribution. Hence, most of the temperature drop occurs in the liquid region. Although the velocity profile (Figures 9 and 10) is nearly symmetric in both axes, the isotherm profiles are not symmetric along the y-axis. Temperature in the upper half of the channel is lower than that at the bottom half. Negative values of the non-dimensional temperature values indicate that the local temperature is lower than the fluid bulk temperature.

The local heat transfer coefficient along the solid-liquid

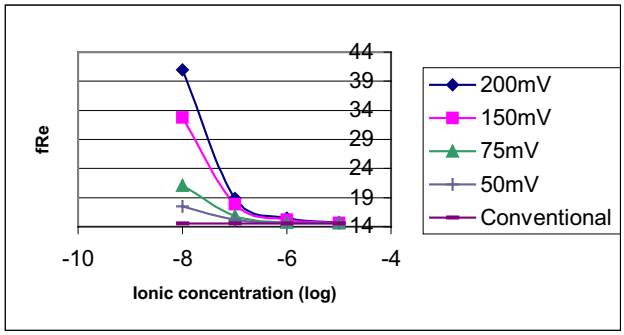

Figure 13 : Graph of f*Re against ionic concentration

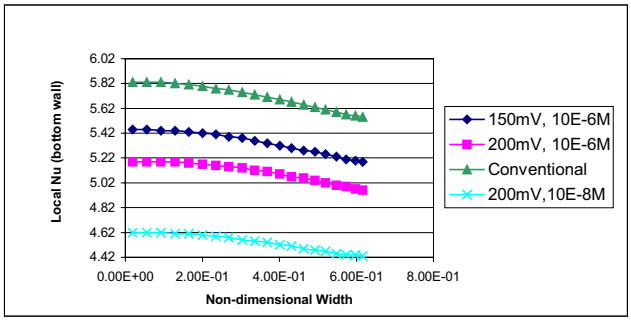

Figure 14 : Variation of local Nusselt Number along the bottom wall

interface is calculated to provide an insight of the overall heat transfer characteristics in the microchannel. Figure 14 shows the variation of the local Nusselt number along the bottom wall of the channel. It is observed that the Nusselt number with the inclusion of EDL is lower than the conventional value. The local Nusselt number decreases towards the edge of the vertical wall until it reaches a minima at the channel corners where the local velocities and their gradients are the smallest.

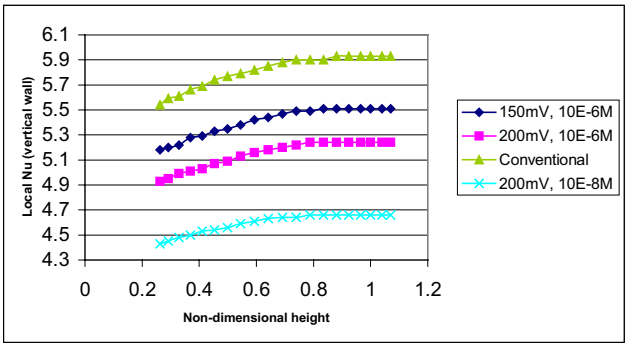

Figure 15 : Variation of local Nusselt Number along the vertical wall

Figure 15 shows the variation of the local Nusselt number along the vertical wall. Inclusion of the EDL also results in the reduction of the local Nusselt number along the vertical wall against the conventional values. The Nusselt number attains constant maximum values in the upper portion of the channel wall. In general, the Nusselt number increases along the channel height.

5.2 Effect of different geometric parameters: aspect ratios

5.2.1 Non-dimensional electrical potential distribution

The electrical potential profiles in microchannels under 2 different sets of aspect ratios and flow conditions were obtained. It is noted that as aspect ratio decreases (smaller channel height), the EDL field is able to extend to a relatively larger portion of the fluid region (not shown here).

5.2.2 Non-dimensional velocity contour distribution

Figures 16 and 17 illustrate the non-dimensional velocity distribution in microchannels with and without EDL considerations under various aspect ratios. Again, the flow profile is significantly affected by the channel geometrical conditions. Large aspect ratio channels give higher velocity values. The flow profile is also affected by the presence of electro-kinetic effects. Stronger EDL effects result in lower velocities.

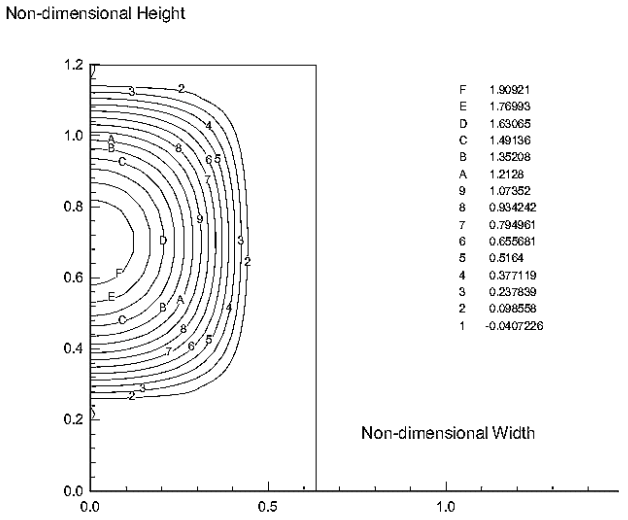

Figure 16 : Non-dimensional velocity distribution, aspect ratio = 1.0 (200mV, 10^{-8}M)

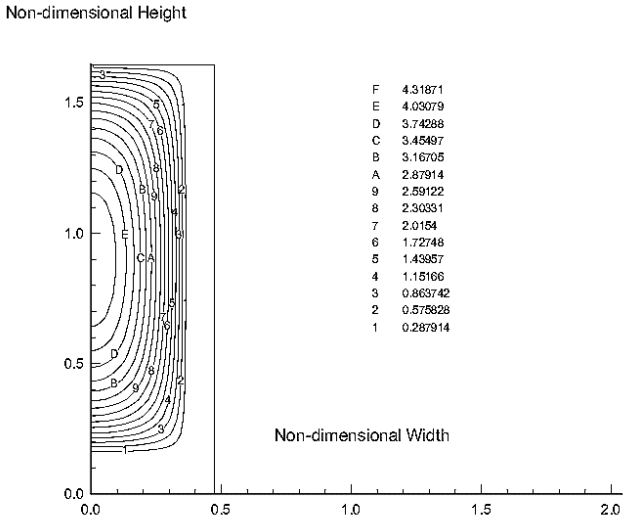

Figure 17 : Non-dimensional velocity distribution, aspect ratio = 2.0 (Conventional)

5.2.3 Non-dimensional temperature contour distribution

Figures 18 and 19 present the non-dimensional temperature contour distribution in microchannels for various geometrical conditions. It is observed that under EDL consideration, the non-dimensional temperature values increased. The stronger the EDL field, the larger the magnitude of temperature increases.

As expected, negligible temperature variations were observed in the solid region due to the large ratio of thermal conductivity between the solid and the liquid. However, in larger aspect ratio channels (Figure 19), slight variations were observed in the fin section of the microchannel heat sink.

6 Conclusion and future works

Interfacial electrokinetic phenomena such as the electric double layer (EDL) play important roles in various transport processes in microchannels. Conventional theories of fluid mechanics and heat transfer cannot explain these phenomena observed in microchannels. The presence of the EDL reduces the liquid velocity within the microchannel, which affects the heat transfer mechanism in the pressure-driven microchannels. In the current study, a source term in the form of the electrical body force was included in the governing momentum equations for microscale computation with the effects of the heat trans-

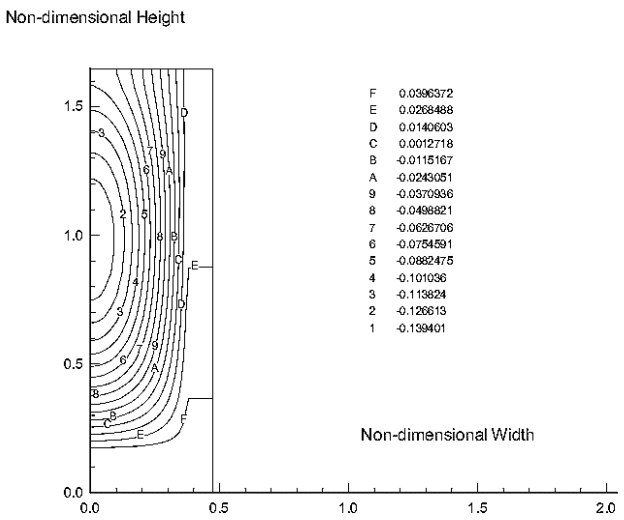

Figure 18 : Non-dimensional temperature distribution, aspect ratio = 2.0 (150mV, 10^{-6}M)

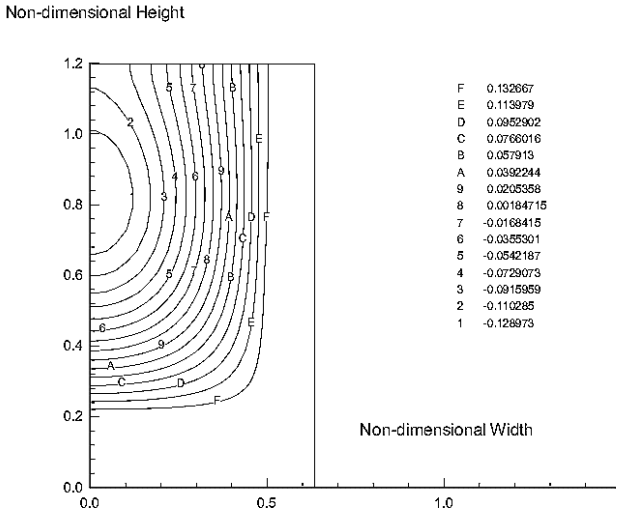

Figure 19 : Non-dimensional temperature distribution, aspect ratio = 1.0 (Conventional)

fer through the channel wall. The numerical parametric studies performed allowed the conclusion that the flow and heat transfer characteristics in microchannels depend on the bulk ionic concentration, the Zeta potential and the aspect ratio of the channel, which is the reflection of the EDL effects. The existing of the EDL is more significant as aspect ratios decreases. Also, the friction coefficient increases as the ionic concentration of the aqueous KCL solution decreases and the zeta potential of the system increases. However, one should be aware that the ionic concentration of 10^{-8} M is unlikely in reality.

The future works may include:

a. The possible application of overlapping EDL fields within the microchannel.

b. Application of EDL analysis to a developing flow.

c. The studies of various kinds of coolants as both gaseous and liquid flows have significant differences on the flow phenomena. The use of different substrates may result in different ranges of zeta potentials.

d. In a traditional microchannel heat sink design (single layer parallel flow), the undesirably high bulk temperature rises along the microchannels could be controlled by increasing the pressure drop across the microchannels. However, this requires a more powerful pumping power supply and this in turn, generates more noise and needs bulkier packaging. Thus, it is worthy to further study the flow in other microchannel arrangements such as:

   i. Single layer microchannels with the coolant flow in the opposite direction in alternate microchannels (counterflow), and,

   ii. Double-layer or multi-layer (stacking) microchannels, with the coolant flow in the opposite direction in each layer.

References

Atluri,SN and Shen, S (2002a): *The meshless local Petrov-Galerkin (MLPG) method*. 440 pages, Tech Science Press.

Atluri,SN and Shen, S (2002b): The meshless local Petrov-Galerkin (MLPG) method: a simple & less-costly alternative to the finite element and boundary element methods, *CMES: Computer Modeling in Engineering & Sciences*, Vol. 3, no. 1, pp. 11-52.

Hunter, R. J. (1981): *Zeta potential in colloid science: principles and applications*. Academic Press, New York.

Kim, H.-G.; Atluri, S.N. (2000): Arbitrary placement of secondary nodes, and error control, in the Meshless Local Petrov-Galerkin (MLPG) method. *CMES: Computer*

Modelling in Engineering & Sciences, Vol. 1, no. 3, pp. 11-32.

Lin, H.; Atluri, S.N. (2000): Meshless Local Petrov-Galerkin (MLPG) method for convection-diffusion problems. *CMES: Computer Modelling in Engineering & Sciences,* Vol. 1, no. 2, pp. 45-60.

Lin, H.; Atluri, S.N. (2001): The Meshless Local Petrov-Galerkin (MLPG) method for solving incompressible NS equations. *CMES: Computer Modelling in Engineering & Sciences,* Vol. 2, no. 2, pp. 117-142.

Mala, G. M.; Li, D.; Dale, J. D. (1997): Heat transfer and fluid flow in microchannels. *Int. J. Heat Mass Transfer*. Vol. 40, no. 13, pp. 3079-3088.

Ng, E. Y-K.; Poh S.T. (1999): Fluid flow and heat transfer in manifold microchannel heat sinks: a CFD approach, *International J. of Computer Modelling and Simulation in Engineering*, Sage Science Press, vol. 4, no. 4, pp. 282-289.

Ngo, N. D.; Tamma, K. K. (2000): Non-isothermal three-dimensional developments and process modeling of composites: flow/thermal/cure formulations and experimental validations. *CMES: Computer Modelling in Engineering & Sciences, vol.* 1, no. 3, pp. 57-72.

Patankar, S.V. (1991): *Computation of conduction and duct flow heat transfer.* Innovative Research Inc., Maple Grove, USA. pp. 67-91.

Probstein R. F. (1994): *Physicochemical hydrodynamics, an introduction.* 2^{nd} Ed.. John Wiley & Sons Ltd.. New York. pp. 161-198.

Shah, R. K.; London, A. L. (1978): *Laminar flow forced convection in ducts.* Academic Press.

Samalam, V. K. (1989): Convective heat transfer in microchannels. *J. of Electronic Materials* vol. 18, no. 5, pp. 611-617.

Tuckerman, D. B,; Pease, R. F. W. (1981): High-performance heat sinking for VLSI. *IEEE Electron Device Letters*, vol. 2, no. 5, pp. 126-129

Weast, R.; Astle, M.J.; Beyer, W.H. (1986): *CRC handbook of chemistry and physics*. CRC Press Inc., Boca Raton.

Weisberg, A.; Bau, H. H.; Zemel, J. N. (1992): Analysis of microchannels for integrated cooling. *Int. J. Heat Mass Transfer*, vol. 35, no. 10, pp. 2465-2474.

Wordelman, C.J.; Aluru, N.R.; Ravaioli, U. (2000): A meshless method for the numerical solution of the 2- and 3-d semiconductor Poisson equation. *CMES: Computer Modelling in Engineering & Sciences, vol.* 1, no. 1, pp. 121-126.

Yang, C.; Li, D. (1997): Electrokinetic effects on pressure-driven liquid flows in rectangular microchannels. *J. Colloid Interface Sci.* vol. 194, pp. 95-107.